Chemistry & Biochemistry Faculty Publications   Chemistry & Biochemistry

Size-Dependent Inhibitory Effects of Antibiotic Nanocarriers on Filamentation of *E. coli*

Preeyaporn Songkiatisak
Old Dominion University

Feng Ding
Old Dominion University

Pavan Kumar Cherukuri
Old Dominion University

Xiao-Hong Nancy Xu
Old Dominion University, xhzu@odu.edu

Check for updates

Size-dependent inhibitory effects of antibiotic nanocarriers on filamentation of *E. coli*

Preeyaporn Songkiatisak, [ID] † Feng Ding, [ID] † Pavan Kumar Cherukuri†
and Xiao-Hong Nancy Xu [ID] *

Multidrug membrane transporters exist in both prokaryotic and eukaryotic cells and cause multidrug resistance (MDR), which results in an urgent need for new and more effective therapeutic agents. In this study, we used three different sized antibiotic nanocarriers to study their mode of action and their size-dependent inhibitory effects against *Escherichia coli* (*E. coli*). Antibiotic nanocarriers (AgMUNH–Oflx NPs) with 8.6×10^2, 9.4×10^3 and 6.5×10^5 Oflx molecules per nanoparticle (NP) were prepared by functionalizing Ag NPs (2.4 ± 0.7, 13.0 ± 3.1 and 92.6 ± 4.4 nm) with a monolayer of 11-amino-1-undecanethiol ($MUNH_2$) and covalently linking ofloxacin (Oflx) with the amine group of $AgMUNH_2$ NPs, respectively. We designed a modified cell culture medium for nanocarriers to be stable (non-aggregated) over 18 h of cell culture, which enabled us to quantitatively study their size and dose dependent inhibitory effects against *E. coli*. We found that the inhibitory effects of Oflx against *E. coli* highly depended upon the dose of Oflx and the size of the nanocarriers, showing that an equal amount of Oflx that was delivered by the largest nanocarriers (92.6 ± 4.4 nm) were most potent with the lowest minimum inhibitory concentration (MIC_{50}) and created the longest and highest percentage of filamentous cells, while the smallest nanocarriers (2.4 ± 0.7) were least potent with the highest MIC_{50} and produced the shortest and lowest percentage of filamentous cells. Interestingly, the same amount of Oflx on 2.4 ± 0.7 nm nanocarriers showed a 2× higher MIC and created 2× shorter filamentous cells than free Oflx, while the Oflx on 13.0 ± 3.1 and 92.6 ± 4.4 nm nanocarriers exhibited 2× and 6× lower MICs, and produced 2× and 3× longer filamentous cells than free Oflx, respectively. Notably, the three different sized $AgMUNH_2$ NPs (absence of Oflx) showed negligible inhibitory effects and did not create filamentous cells. The results show that the filamentation of *E. coli* highly depends upon the sizes of nanocarriers, which leads to the size-dependent inhibitory effects of nanocarriers against *E. coli*.

Introduction

Antibiotics have been widely used to treat infectious diseases for years. Multi-antibiotic resistance has led to ineffectiveness of conventional antibiotics, creation of super bugs and an urgent need for new antibiotics to treat infectious diseases. Multidrug membrane transporters exist in both prokaryotes and eukaryotes, and they can selectively extrude structurally and functionally unrelated substrates out of the cells to keep the intracellular drug concentration low, which leads to low efficacy of therapeutic agents.[1–6] Thus, multidrug membrane transporters have been extensively studied over decades and they have been selected as drug targets to overcome MDR and improve the efficacy of therapeutic drugs. However, despite

extensive studies, molecular mechanisms and functions of multidrug membrane transporters remain elusive.[7,8]

Escherichia coli (*E. coli*) is a Gram-negative bacterium and can cause severe diarrhea, urinary tract infections and respiratory illness.[9,10] There are several multidrug membrane transporters in *E. coli*.[11–13] For instance, the MsbA in *E. coli* is a well-known multidrug ATP-binding cassette (ABC) transporter that is closely related to other multidrug membrane transporters (*e.g.*, Pgp, ABCB1, and MDR1) in eukaryotes.[11–13] MsbA shares a common modular architecture with other ABC transporters and consists of two transmembrane domains (TMDs) that define substrate binding-sites and form the transport passageway for substrates to cross the cellular membrane, and two nucleotide-binding domains (NBDs) that bind and hydrolyze ATP to provide the "power-stroke" for the transporter to translocate specific substrates across the cellular membrane.[14–20] Studies have shown that MsbA uses both ATP and proton gradients across the cellular membrane as energy sources to extrude pump substrates out of cells.[21]

Department of Chemistry and Biochemistry, Old Dominion University, Norfolk, Virginia 23529, USA. E-mail: xhxu@odu.edu; Web: http://www.odu.edu/~xhxu; Fax: +1 (757) 683 5698; Tel: +1 (757) 683 5698

† These authors contributed equally to this work.

Extensive efforts have been made to study and overcome MDR mediated by multidrug efflux pumps. Polymer-based NPs have been used to increase the drug payload and to increase the efficacy of therapeutic agents.[22–25] Other NPs themselves have showed inhibitory effects against bacteria.[26,27] However, the dependence of their efficacy and inhibitory effects upon their physicochemical properties has not yet been systematically studied, which hinders rational design of drug nanocarriers to effectively overcome MDR and to effectively achieve their maximum efficacy. Noble metal NPs (*e.g.* Ag and Au NPs) possess distinctive plasmonic optical properties, superior photostability and well characterized size, shape and surface properties. Thus, they can serve as a model system to study the size-dependent inhibitory effects of drug nanocarriers and serve as imaging probes to track their distributions and study their mode of actions against cells. We have demonstrated that we can image and characterize the sizes of single Ag NPs at nanometer (nm) resolution in single live cells *in situ* in real time using size-dependent localized surface plasmon resonance (LSPR) spectra of single Ag NPs by dark-field optical microscopy and spectroscopy (DFOMS).[28–44] We have used the size-dependent LSPR spectra of single Ag NPs to track the transport of single NPs in and out of single live cells and to determine the pore sizes of membrane transporters.[29,30]

In our previous studies, we found dose and size dependent inhibitory effects of antibiotic nanocarriers (AgMUNH–Oflx NPs) against *Pseudomonas aeruginosa* (Gram-negative bacterium) and *Bacillus subtilis* (Gram-positive bacterium).[45,46] Interestingly, we found that inhibitory effects of antibiotic nanocarriers highly depended upon the expression of MexAB-OprM (a multidrug ABC membrane transporter in *Pseudomonas aeruginosa*),[46] but not the expression of BmrA (a multidrug membrane transporter) in *Bacillus subtilis*.[45] In this study, we used the exactly same antibiotic nanocarriers to study the dose and size dependent inhibitory effects of nanocarriers against *E. coli* (Gram-negative bacterium), and used an ATPase inhibitor (orthovanadate) to inhibit ABC transporters in *E. coli*, aiming to study the mode of action of nanocarriers and the dependence of inhibitory effects of nanocarriers upon ABC transporters and the bacterial strain.

Materials and methods

Reagents and the cell line

Silver nitrate (99.9%), sodium citrate dehydrate (99%), sodium borohydride (98%), hydrogen peroxide (30%), poly-vinylpyrrolidone (PVP), 2-mercaptoethanol (99%), 11-amino-1-undecanethiol hydrochloride (MUNH₂, 99%), ofloxacin powder (99%), orthovanadate (≥90%), sodium chloride, sodium phosphate, sodium phosphate monobasic monohydrate, Bacto-Tryptone, and Bacto Yeast Extract were purchased from Sigma-Aldrich. *N*-Hydroxysulfosuccinimide (Sulfo-NHS, 98.5%, Pierce), 1-ethyl-3-[3-dimethylaminopropyl]-carbodiimide hydrochloride (EDC, 99%, Pierce), silver perchlorate monohydrate (99%, Alfa Aesar), live/dead backlight viability assay (Life Technologies), and Hoechst 33342 (Life Technologies) were purchased as indicated, and used as received. The cell line

of *Escherichia coli* (wt w3110) was purchased from a genetic stock center (CGSC). Deionized (DI) water (18 MΩ water, Barnstead) was used to prepare all the solutions including a standard LB medium (1% tryptone peptone, 0.5% yeast extract, and 0.5% NaCl, pH = 7.2) and a modified LB medium (1% tryptone peptone, 0.5% yeast extract, and 0.1% NaCl, pH = 7.2).

Synthesis and characterization of antibiotic nanocarriers

We synthesized, purified and characterized three different sized antibiotic nanocarriers with diameters of Ag NPs of (2.4 ± 0.7), (13.0 ± 3.1) and (92.6 ± 4.4) nm and the molar conjugation ratios of antibiotics (Oflx) per NP of 8.6×10^2, 9.4×10^3, and 6.5×10^5, respectively, as we reported previously.[46] We first synthesized, purified and characterized the three different sized Ag NPs, as we reported previously.[28,30,34,37,47,48] We characterized the NP concentrations, the plasmonic optical properties (LSPR images and spectra), sizes and zeta potentials of single NPs using UV-Vis absorption spectroscopy (Hitachi U-2010), dark-field optical microscopy and spectroscopy (DFOMS), high-resolution transmission electron microscopy (HRTEM) (JEOL, JEM-2100F), and dynamic light scattering (DLS) (Nicomp 380ZLS particle sizing system), respectively.[28,30,34,37,47,48]
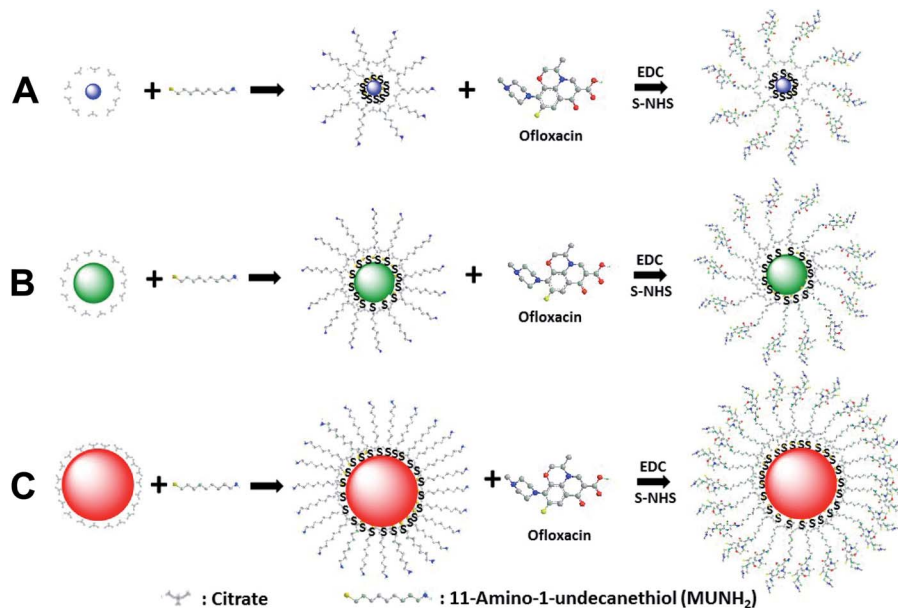
We used the interaction of thiol groups of MUNH₂ with the NPs to directly attach 11-amino-1-undecanethiol hydrochloride (MUNH₂) onto the surface of NPs and create AgMUNH₂ NPs.[46] We removed excess MUNH₂ by thoroughly washing the AgMUNH₂ NPs with DI water three times using centrifugation (Beckman Optima L90k, 4 °C). We then covalently conjugated the carboxyl group of Oflx with the amine groups of MUNH₂ attached onto the surface of the NPs (AgMUNH₂ NPs) *via* the peptide bond to prepare antibiotic nanocarriers (AgMUNH–Oflx NPs) using a two-step method *via* EDC and s-NHS as mediators (Fig. 1). We thoroughly washed the drug nanocarriers with DI water three times and stored them at 4 °C for future use.

We characterized the concentrations, optical properties and sizes of the nanocarriers using UV-Vis absorption spectroscopy, DFOMS and DLS, respectively. We determined the molar concentration of NPs and Oflx attached on the NPs for each different sized nanocarrier by measuring the plasmonic absorption spectra of the NPs and the absorbance spectra of Oflx at 288 nm, respectively.[46] We then divided the molar concentrations of Oflx molecules on the surface of the nanocarriers by the molar concentration of the NPs, to determine the molar conjugation ratios of Oflx molecules/ NP for each different sized nanocarrier. We studied the stability of each different sized nanocarrier (AgMUNH–Oflx NPs) in the standard (1% tryptone peptone, 0.5% yeast extract, and 0.5% NaCl, pH = 7.2) and modified LB medium (1% tryptone peptone, 0.5% yeast extract, and 0.1% NaCl, pH = 7.2) over 24 h using UV-Vis absorption spectra, DLS and DFOMS.

Design of the cell culture medium and characterization of cultured cells

We studied the cell growth of the *E. coli* strain in the standard and the modified LB medium in parallel. We first pre-cultured
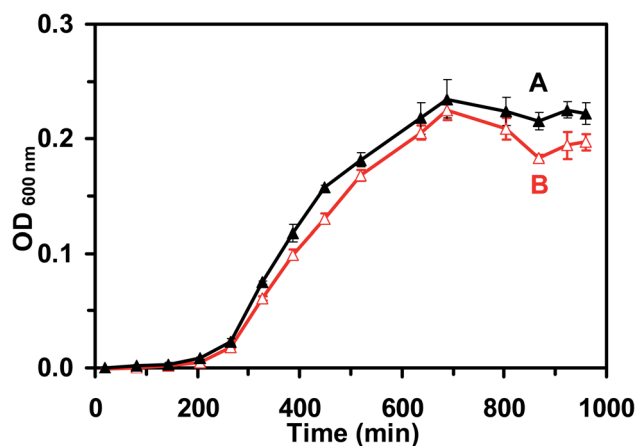
Fig. 1 Chemical reactions of synthesis of antibiotic nanocarriers. Functionalization of Ag NPs with a self-assembled monolayer of 11-amino-1-undecanethiol (MUNH$_2$) by interaction of its thiol groups (–SH) with the surface of Ag NPs with diameters of (A) 2.4 ± 0.7, (B) 13.0 ± 3.1 and (C) 92.6 ± 4.4 nm to synthesize AgMUNH$_2$ NPs. The amine groups of AgMUNH$_2$ NPs were covalently conjugated with the carboxyl groups of ofloxacin (Oflx) *via* the peptide bond using EDC and sulfo-NHS as mediators to produce AgMUNH–Oflx NPs, which we named as antibiotic nanocarriers.[46]

the cells in a standard LB medium in a floor shaker (Thermo Scientific, MaxQ5000) (200 rpm, 37 °C) for 12 h. We then cultured the cells in either the standard LB medium or the modified LB medium in the shaker (200 rpm, 37 °C) for another 8 h. We followed the cell growth in each medium over time and characterized the cell growth curves by measuring OD$_{600\text{ nm}}$ of the cell suspension every 6 h over 18 h (Fig. 2). The cell suspension was diluted 10× and measured with an OD$_{600\text{ nm}}$

Fig. 2 Study of the growth kinetics of the live cells (*E. coli*) cultured in (A) standard and (B) modified LB medium. The cell growth curves of *E. coli* in the (A) standard and (B) modified LB medium show that the growth rates of the cells cultured in either medium are nearly identical, which indicates that the cells in the modified LB medium grew normally. Each cell suspension was diluted 10× and measured at OD$_{600\text{ nm}}$ below 0.25.

below 0.25, in order to ensure that the cell concentration can be determined using OD$_{600\text{ nm}}$. Finally, by the end of cell culture at 18 h, we characterized the viability of the cultured cells at single-cell resolution using live/dead *Bac*Light viability and counting assay (Fig. 3).[49] We imaged the cells in a micro-chamber using dark-field optical microscopy and epi-fluorescence microscopy and counted the green fluorescent cells (peak wavelength of fluorescence spectra of SYTO9, λ_{max} = 520 nm) and the red fluorescent cells (peak wavelength of fluorescence spectra of propidium iodide, λ_{max} = 610 nm) as live and dead cells, respectively.[29,44,46,49]

We further characterized the efflux function of the ABC membrane transporter of the cells cultured in the standard and the modified LB medium by measuring the time-course of the fluorescence intensity of the dye (Hoechst 33342) accumulated inside the cells in the presence and absence of the ATPase inhibitor (orthovanadate) using fluorescence spectroscopy, as described in the following.[29,50,51] We harvested the cultured cells using centrifugation (Beckman Model J2-21 Centrifuge, JA-14 rotor, at 7500 rpm, 23 °C, 10 min), thoroughly washed the cells with the PBS buffer (0.5 mM phosphate buffer, 1.5 mM NaCl, pH 7.2) three times, and resuspended the cells in the buffer. The final concentration of the cells was adjusted to OD$_{600\text{ nm}}$ = 0.1. The time-course fluorescence intensity of Hoechst 33342 (0.5 µM) incubated with the cells in the presence and absence of orthovanadate (25 µM) was measured at a 10 s data acquisition interval in real time using a fluorescence spectrometer (PerkinElmer LS50B) (Fig. 4). The excitation and emission wavelengths were 354 and 478 nm, respectively.
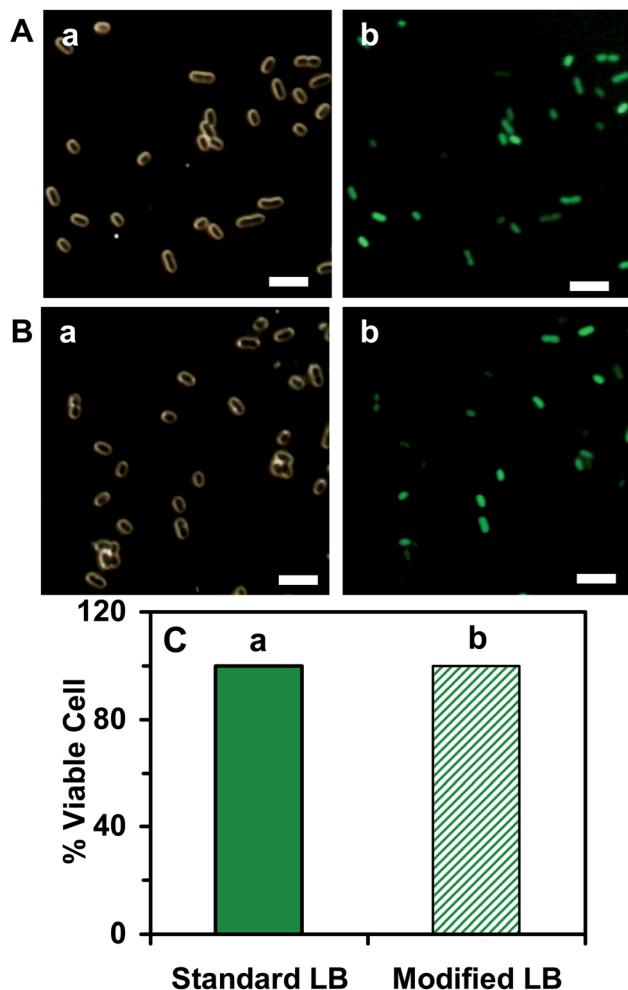
Fig. 3 Characterization of the viability of the *E. coli* cells cultured in the (A) standard and (B) modified LB medium using the live/dead *Bac*Light assay: (a) optical images and (b) fluorescence images of single *E. coli* cells that were cultured in the medium over 18 h and characterized by live/dead *Bac*Light assay. The live cells emit the green fluorescence ($\lambda_{max} = 525$ nm) of SYTO9 and the dead cells emit the red fluorescence ($\lambda_{max} = 608$ nm) of propidium iodide. (C) Plot of the percentage of the live cells (number of live cells divided by the total number of cells) cultured in the (a) standard and (b) modified LB medium shows that more than 99% of the cells are viable, indicating that the modified LB medium is well suitable for culturing the viable cells. Minimum 900 cells for each medium were assayed. The scale bars in (A and B) are 5 μm.

Study of size-dependent inhibitory effects of antibiotic nanocarriers against *E. coli*

We cultured the cells (10^4 pre-cultured cells) in the modified LB medium (3.0 mL) containing a dilution series of free Oflx and Oflx attached onto the given sized drug nanocarrier in a shaker (MaxQ5000) under vigorous shaking (200 rpm, 37 °C) over 18 h. The dilution series consist of (a) 0, (b) 0.045, (c) 0.09, (d) 0.18, (e) 0.38, and (f) 0.68 μM free Oflx (Fig. 5A(a–f)) or the same concentrations of Oflx attached onto the nanocarriers which correspond to the concentrations of (Fig. 5B): (a) 0.79 nM AgMUNH$_2$ NPs (in the absence of Oflx, control), and
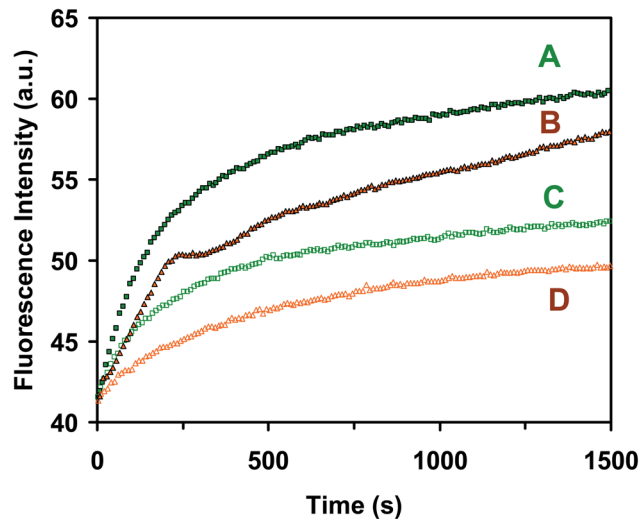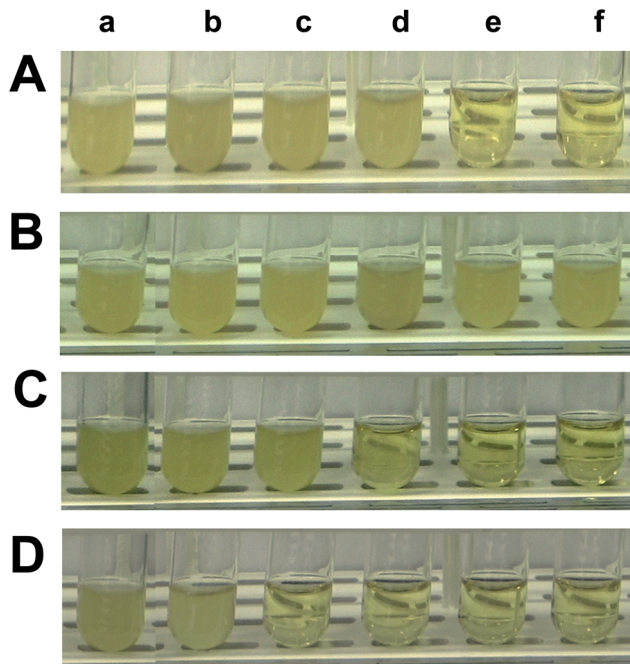

Fig. 4 Characterization of the efflux function of ABC transporters of the *E. coli* cells cultured in the standard (A and C) and modified (B and D) medium, and (A & B) in the presence of 25 μM orthovanadate (inhibitor of ATPase) and (C & D) in the absence of the inhibitor. Time-course fluorescence intensity of Hoechst 33342 (0.5 μM) incubated with the cells (OD$_{600\ nm}$ = 0.1 in PBS buffer, pH 7.2): (A and B) in the presence of 25 μM orthovanadate and (C and D) in the absence of the inhibitor for the cells cultured the in standard (A & C) and modified (B & D) medium shows that the ABC transporters of the cells cultured in the standard (A and C) and modified (B and D) medium exhibit similar efflux kinetics, which demonstrates that the modified LB medium is well suitable to culture the cells for study of the efflux function of ABC membrane transporters.

nanocarriers (NP concentrations): (b) 5.2×10^{-2}, (c) 0.10, (d) 0.21, (e) 0.44, and (f) 0.79 nM for 2.4 ± 0.7 nm NPs with a molar conjugation ratio of 8.6×10^2 Oflx molecules per NP; (Fig. 5C): (a) 7.2×10^{-2} nM AgMUNH$_2$ NPs (in the absence of Oflx, control), and nanocarriers (NP concentrations): (b) 4.8×10^{-3}, (c) 9.5×10^{-3}, (d) 1.9×10^{-2}, (e) 4.0×10^{-2}, and (f) 7.2×10^{-2} nM for 13.0 ± 3.1 nm NPs with a molar conjugation ratio of 9.4×10^3 Oflx molecules per NP; and (Fig. 5D): (a) 1.0 pM AgMUNH$_2$ NPs (in the absence of Oflx, control), and nanocarriers (NP concentrations): (b) 6.9×10^{-2}, (c) 0.14, (d) 0.28, (e) 0.58, and (f) 1.0 pM for 92.6 ± 4.4 nm NPs with a molar conjugation ratio of 6.5×10^5 Oflx molecules per NP. The experiments and controls were carried out in parallel and under the same conditions.

We sampled the cell suspensions every 6 h, diluted each suspension 10× using the medium and then quantitatively determined the bacterial cell concentration by measuring the optical density at 600 nm (OD$_{600\ nm}$) in a 96-well plate using a plate reader (BioTek SynergyHT) equipped with an UV-Vis absorption spectral detector. We plotted the OD$_{600\ nm}$ of the cell suspension over time to determine the time (18 h) for the cultured cells to reach their confluence. Thus, we used the OD$_{600\ nm}$ of each cell suspension at 18 h to determine the inhibitory effects of the free Oflx and Oflx nanocarriers (Fig. 6). We also imaged the number and morphologies of single cells of each cell suspension in a microchamber using dark-field optical microcopy every 6 h over 18 h (Fig. 7).
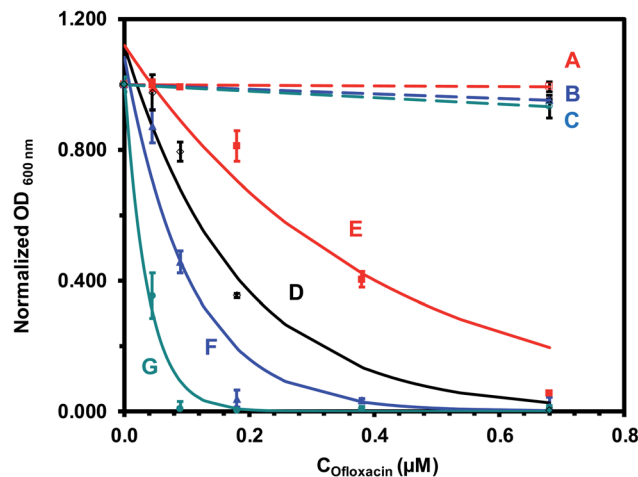
Fig. 5 Study of dose and size dependent inhibitory effects of antibiotic nanocarriers (AgMUNH–Oflx NPs) against the growth of the *E. coli* cells. The cells were cultured in the modified medium containing: (A) free Oflx alone at (a) 0 (blank control), (b) 0.045, (c) 0.09, (d) 0.18, (e) 0.38 and (f) 0.68 µM; (B–D) antibiotic nanocarriers of (B) 2.4 ± 0.7, (C) 13.0 ± 3.1 and (D) 92.6 ± 4.4 nm with (a) 0 (AgMUNH$_2$ NPs, without Oflx), (b) 0.045, (c) 0.09, (d) 0.18, (e) 0.38 and (f) 0.68 µM Oflx. The concentrations of AgMUNH$_2$ NPs in (a) containing the same concentration of the NPs as that of the highest concentration of each different sized nanocarrier in ((f) in B–D): 0.79 nM, 7.2 × 10^{-2} nM and 1.0 pM NPs, respectively.

Fig. 6 Quantitative analysis of size-dependent MIC$_{50}$ of antibiotic nanocarriers (AgMUNH–Oflx NPs) against the *E. coli* cells in Fig. 5. Plots of normalized OD$_{600\ nm}$ of the cells cultured for 18 h in the modified medium containing (A–C) AgMUNH$_2$ NPs (absence of Oflx, control), (D) free Oflx alone, and (E–G) antibiotic nanocarriers of (E) 2.4 ± 0.7, (F) 13.0 ± 3.1 and (G) 92.6 ± 4.4 nm, *versus* (A–C) AgMUNH$_2$ NP concentration (control of the highest concentration of each different sized nanocarrier), and (D–G) *versus* Oflx concentration. The concentrations of AgMUNH$_2$ NPs in (A–C) containing the same concentration of the NPs as that of the highest concentration of each different sized nanocarrier as 0.79 nM, 7.2 × 10^{-2} nM and 1.0 pM NPs for 2.4 ± 0.7, 13.0 ± 3.1 and 92.6 ± 4.4 nm nanocarriers, respectively. The points are experimental data and each solid line is generated by fitting of the experimental data with an equation ($y = ae^{-bx}$) as the following: (D) $y = 1.12e^{-5.57x}$, $R^2 = 0.944$; (E) $y = 1.12e^{-2.56x}$, $R^2 = 0.928$; (F) $y = 1.08e^{-9.58x}$, $R^2 = 0.941$; and (G) $y = 1.01e^{-26.7x}$, $R^2 = 0.988$. Concentrations of Oflx (MIC$_{50}$, IC$_{50}$) for free Oflx and given sized nanocarriers were determined using the exponential fitting equation at the half of the maximum of the normalized OD$_{600\ nm}$, respectively.

The MIC can be determined by culturing the bacterial cells in the dilution series of antibiotics either in a liquid LB-medium or on solid culture plates (CFU, a colony-forming unit). In this study, we cultured the bacterial cells in the dilution series of antibiotics in a liquid LB-medium, which enabled the nanocarriers to be well dispersed and avoided the aggregation of nanocarriers in solid culture plates. Furthermore, this enabled us to characterize the stability of nanocarriers in the liquid medium in real time at single NP resolution, and to determine the MICs semi quantitatively by mathematically fitting the experimental data.

Data analysis and statistics

We characterized sizes and shapes of single Ag NPs using TEM, and LSPR spectra of single Ag, AgMUNH$_2$, and AgMUNH–Oflx NPs using DFOMS, as we reported previously.[46] We imaged at least 100 NPs for each measurement and repeated each experiment three times for each individual size. Therefore, a minimum of 300 NPs were characterized using TEM and DFOMS. All the experiments were carried out in triplicate for each concentration and each different sized antibiotic nanocarriers. We used the average of three measurements with standard deviations to characterize the size-dependent inhibitory effects of nanocarriers on the cell growth.

Results and discussion

Antibiotic nanocarriers (AgMUNH–Oflx NPs)

To study the dependence of inhibitory effects upon the bacterial strains and enable us to compare this study with previous studies, we used the same antibiotic nanocarriers as those that we designed, synthesized and characterized in our previous studies.[45,46] We first synthesized, purified and characterized three different sized Ag NPs with diameters of 2.4 ± 0.7, 13.0 ± 3.1 and 92.6 ± 4.4 nm. We used the strong interaction of the thiol of 11-amino-1-undecanethiol hydrochloride (MUNH$_2$) with the surface of Ag NPs to attach a self-assembled monolayer of MUNH$_2$ onto the NPs and to create AgMUNH$_2$ NPs (Fig. 1).[45,46] We then covalently linked the carboxyl group of Oflx with the amine group of MUNH$_2$ on the NPs (AgMUNH$_2$ NPs) using the peptide bond to produce antibiotic nanocarriers (AgMUNH–Oflx NPs) (Fig. 1).[45,46]

We thoroughly washed the nanocarriers with DI water using centrifugation to remove unattached antibiotics and chemicals and to purify the nanocarriers. We characterized the sizes and optical properties of the Ag NPs, AgMUNH$_2$ NPs and AgMUNH–Oflx NPs using TEM, DLS and DFOMS. We quantitatively
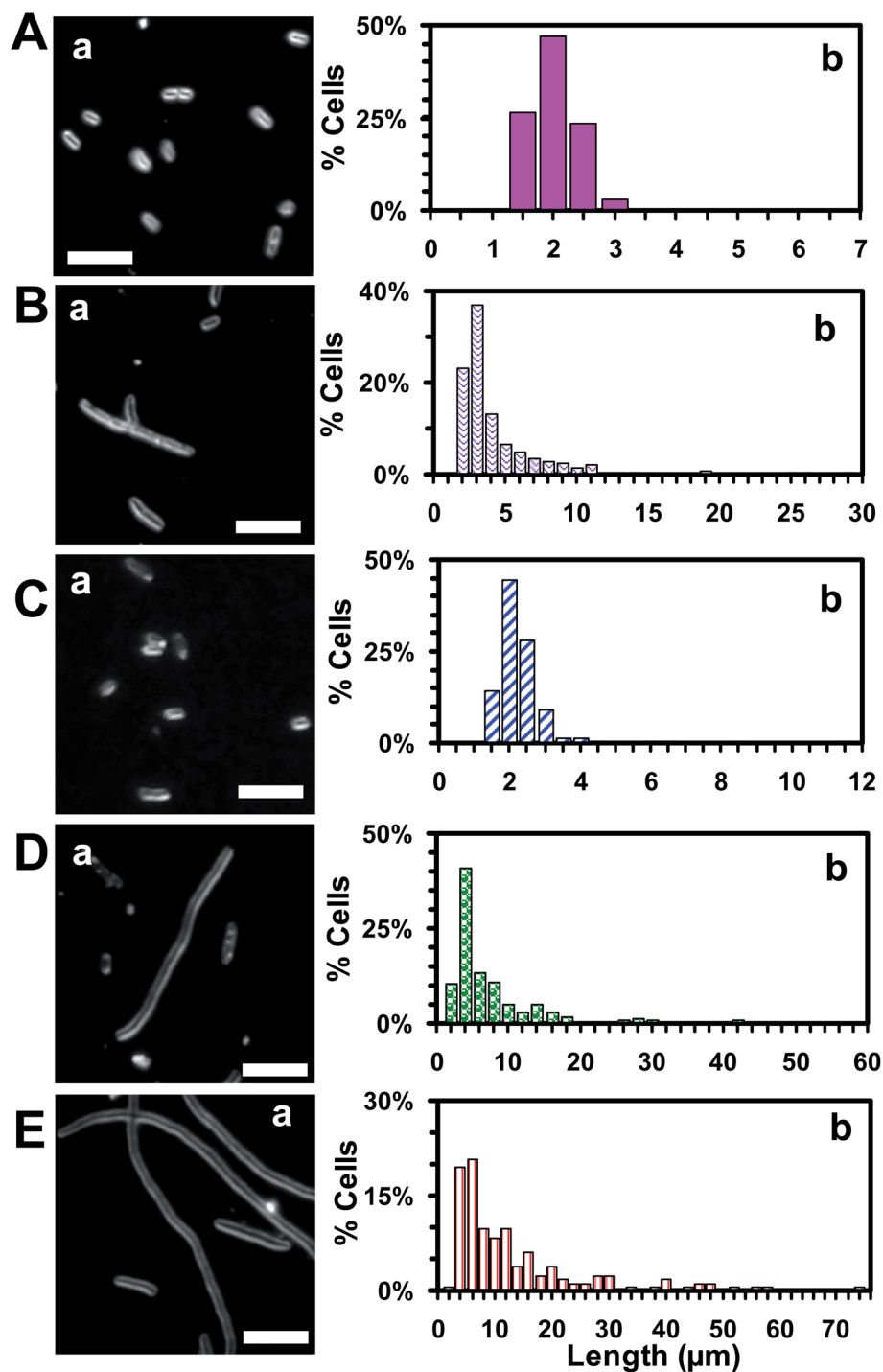
Fig. 7 Study of dependence of bactericidal inhibitory effects (morphology and length of single *E. coli* cells) of antibiotic nanocarriers upon their sizes. Representative (a) dark-field optical images and (b) histograms of distribution of length of single cells that were cultured for 18 h in the modified medium containing (A) 0 (blank control), (B) 0.045 μM free Oflx alone, and (C–E) 0.045 μM Oflx attached onto the NPs (antibiotic nanocarriers) with diameters of: (C) 2.4 ± 0.7, (D) 13.0 ± 3.1 and (E) 92.6 ± 4.4 nm, show the size-dependent bactericidal inhibitory effects of the antibiotic nanocarriers and that the largest nanocarriers create the highest bactericidal inhibitory effects and generate the longest filamentation and highest percentage of filamentous cells. The scale bars in (a) are 5 μm.

determined the molar conjugation ratios of Oflx molecules per NP for 2.4 ± 0.7, 13.0 ± 3.1, and 92.6 ± 4.4 nm NPs to be 8.6 × 10^2, 9.4 × 10^3, and 6.5 × 10^5 using UV-Vis absorption spectra of the plasmonic absorption of the given sized NPs and absorption of Oflx at 288 nm, respectively.[46] We also characterized the zeta potentials of Ag NPs, Ag MUNH$_2$ NPs and AgMUNH–Oflx NPs in PBS buffer (pH 7.2) using a Nicomp 380ZLS particle sizing system, as summarized in Table 1. The citrate molecules (pK_{a1}

Table 1 Characterization of zeta potentials of Ag, AgMUNH₂, and AgMUNH–Oflx NPs (nanocarriers) in the PBS buffer (pH = 7.2)

Size (nm)	Zeta potentials (mV)		
	Ag NPs	AgMUNH₂ NPs	AgMUNH–Oflx NPs
2.4 ± 0.7	−21.38	2.35	2.11
13.0 ± 3.1	−33.52	8.82	7.57
92.6 ± 4.4	−55.16	21.26	18.14

= 3.31; pK_{a2} = 4.76; pK_{a3} = 6.39) adsorbed onto the NPs in the PBS buffer (pH = 7.2) lead to negatively charged Ag NPs. As MUNH₂ molecules replaced citrate molecules to attach onto the surface of the NPs *via* the interaction of the –SH group with the surface of Ag NPs, positively charged AgMUNH₂ NPs were obtained. The pK_{a1} and pK_{a2} of Oflx were 5.97 and 9.28, respectively.[52] The carboxyl group of the Oflx (pK_{a1}) was covalently linked with the amine group of MUNH₂ attached on the NPs (AgMUNH₂ NPs). Thus, the amine group of Oflx (pK_{a2} of Oflx = 9.28) generated positively charged nanocarriers in the PBS buffer (pH = 7.2), as summarized in Table 1. The charges of the nanocarriers increase with the size of the NPs unproportionally, which is because the surface of the NPs (13.0 ± 3.1 and 92.6 ± 4.4 nm) is not fully covered with Oflx, as indicated by the conjugation ratio of Oflx molecules per NP.[50]

We characterized the stability (non-aggregation) of the antibiotic nanocarriers with desired concentrations in a commonly used standard LB medium (1% tryptone, 0.5% yeast extract and 0.5% NaCl in DI water, pH = 7.2) in the shaker (200 rpm, 37 °C) over 12 h using DLS, UV-Vis spectroscopy and DFOMS. We found that they were aggregated in the standard LB medium, which would alter their sizes, lead to precipitation of the nanocarriers and decrease their doses over time.[46] Therefore, we reduced NaCl concentration from 0.5% to 0.1%, and designed a modified cell culture medium (1% tryptone, 0.5% yeast extract and 0.1% NaCl in DI water, pH = 7.2), in which the nanocarriers with desired concentrations were stable (non-aggregated) over 24 h, under the cell culture conditions, in the shaker (200 rpm, 37 °C).

Viability and efflux function of cells cultured in the modified medium

To characterize the suitability of the modified LB medium for culturing the *E. coli* strain, we followed the cell growth and determined the cell growth kinetics of the cultured cells in both the standard LB medium and the modified LB medium over time. The growth curves of the cells cultured in the standard LB medium (Fig. 2A) and in the modified LB medium (Fig. 2B) over time show the same growth kinetics, indicating that the cells grew well in both mediums. We then characterized the viability of the cells cultured in the standard and the modified medium over 18 h using a live/dead *Bac*Light assay.[49] Representative optical images of the cells cultured in the standard LB medium (Fig. 3A) and the modified LB medium (Fig. 3B) show SYTO9 green fluorescence but not propidium iodide red fluorescence,

demonstrating that more than 99% of the cultured cells were viable (Fig. 3C) and the modified LB medium can be used to culture the cells.

Furthermore, we characterized the efflux functions of the ABC membrane transporters of the live cells (*E. coli*) by measuring the time-course intracellular fluorescence intensity of Hoechst dye (Hoechst 33342) in real time in the presence and absence of the ATPase inhibitor (orthovanadate), which inhibits ATPase and hydrolysis of ATP to ADP that powers the ABC membrane transporters to extrude the substrates out of the cells.[53,54] Notably, the Hoechst dye emits weak fluorescence in aqueous solution and its fluorescence quantum yield increases substantially (up to 10 times) once it enters the cells and intercalates with DNA.[55] The Hoechst dye is a well-known substrate of ABC membrane transporters and has been widely used as an assay for real-time monitoring accumulation of the intracellular dye molecules and for characterization of the efflux kinetics of ABC membrane transporters of live cells.[29,50,51]

The time-course fluorescence intensity of Hoechst dye incubated with the cells that were cultured in the standard LB medium (Fig. 4A) and the modified LB medium (Fig. 4B) in the presence of the ATPase inhibitor (25 μM orthovanadate)[53,54] shows similar accumulation kinetics of intracellular dye molecules. The time-course fluorescence intensity of the dye incubated with the cells that were cultured in the standard LB medium (Fig. 4C) and the modified LB medium (Fig. 4D) in the absence of the ATPase inhibitor (control experiment) shows similar accumulation kinetics of the intracellular dye molecules in the cells cultured in both mediums. The result shows that the fluorescence intensity of the dye incubated with the cells increases with time much more rapidly in the presence of the inhibitor than in the absence of inhibitor, indicating that the ABC transporters extrude the dye molecules out of the cells in the absence of the inhibitor, which leads to the lower and slower accumulation of intracellular dye molecules over time. Taken together, the results in Fig. 2–4 demonstrate that the modified LB medium is well suitable to culture the *E. coli* cells with well-functional ABC membrane transporters.

Size and dose dependent inhibitory effects of antibiotic nanocarriers

We quantitatively determined the size and dose dependent inhibitory effects (MIC₅₀) of Oflx nanocarriers against the *E. coli* cells. We cultured the cells (10⁴ pre-cultured cells) in the modified LB medium containing a dilution series of free Oflx, each given sized Oflx nanocarriers (AgMUNH–Oflx NPs) and the corresponding size AgMUNH₂ NPs (absence of Oflx, control experiment) under vigorous shaking (200 rpm, 37 °C), and measured the cell growth curves over 18 h. The dilution series consist of (a) 0, (b) 0.045, (c) 0.09, (d) 0.18, (e) 0.38, and (f) 0.68 μM free Oflx (Fig. 5A(a–f)) or Oflx attached onto the nanocarriers (Fig. 5B–D(a–f)), respectively. The nanocarriers correspond to (Fig. 5B(a–f)): (a) 0.79 nM AgMUNH₂ NPs (absence of Oflx, control), (b) 5.2×10^{-2}, (c) 0.10, (d) 0.21, (e) 0.44, and (f) 0.79 nM 2.4 ± 0.7 nm nanocarriers with a conjugation ratio of 8.6×10^2 Oflx molecules per NP; (Fig. 5C(a–f)): (a) 7.2×10^{-2} nM

AgMUNH$_2$ NPs (absence of Oflx, control), (b) 4.8×10^{-3}, (c) 9.5×10^{-3}, (d) 1.9×10^{-2}, (e) 4.0×10^{-2}, and (f) 7.2×10^{-2} nM 13.0 ± 3.1 nm nanocarriers with a conjugation ratio of 9.4×10^3 Oflx molecules per NP; (Fig. 5D(a–f)): (a) 1.0 pM AgMUNH$_2$ NPs (absence of Oflx, control), (b) 6.9×10^{-2}, (c) 0.14, (d) 0.28, (e) 0.58, and (f) 1.0 pM 92.6 ± 4.4 nm nanocarriers with a conjugation ratio of 6.5×10^5 Oflx molecules per NP. The cloudy suspensions in Fig. 5 show that the bacterial cells grew, while the clear suspensions indicate that the cell growth was significantly inhibited or the cells did not grow at all, suggesting high dependence of inhibitory effects upon the dose of Oflx and the size of nanocarriers.

We quantitatively determined the concentration of the cells over time by measuring their OD$_{600\ nm}$ (optical density at 600 nm) at 6, 12 and 18 h. We subtracted OD$_{600\ nm}$ of the nanocarriers or AgMUNH$_2$ NPs in the medium (in the absence of the cells) from the OD$_{600\ nm}$ of the cell suspension with the nanocarriers or AgMUNH$_2$ NPs, to determine the cell concentration, respectively. The subtracted OD$_{600\ nm}$ of the cell suspension at 18 h was plotted *versus* the concentration of free Oflx or Oflx covalently conjugated with a given sized Oflx nanocarrier to quantitatively determine the MIC$_{50}$ of Oflx against the *E. coli* (Fig. 6).

Control experiments (Fig. 6A–C) show that the OD$_{600\ nm}$ of the cell suspension incubated with each of the three different sized AgMUNH$_2$ NPs (absence of Oflx, 2.4 ± 0.7, 13.0 ± 3.1 or 92.6 ± 4.4 nm) was nearly independent of size and dose of the NPs, and the cells grew normally as those cultured in the medium alone, indicating that the AgMUNH$_2$ NPs at the given concentrations did not create significant inhibitory effects against the growth of the *E. coli* cells. Note that Ag NPs themselves have showed inhibitory effects against bacteria.[26,32,56] The biocompatibility of the functionalized Ag NPs (AgMUNH$_2$ NPs) could be attributed to the surface protecting layer of MUNH$_2$ and the low concentration of AgMUNH$_2$ NPs, as we reported previously.[33,40,57] At a low concentration, Ag NPs and functionalized Ag NPs do not inhibit bacterial growth and can be used to study the efflux function of single live bacterial cells.[29–32,58,59] Further, our previous studies also show that the positively charged peptide functionalized Ag NPs are more biocompatible with the zebrafish embryonic development than negatively charged peptide functionalized Ag NPs.[57]

In contrast, the OD$_{600\ nm}$ of the cell suspension incubated with free Oflx (Fig. 6D) or Oflx attached onto the given sized nanocarriers (Fig. 6E–G) decreases as Oflx concentration increases and as the size of the nanocarriers increases, showing that inhibitory effects on the growth of *E. coli* cells highly depend upon the dose of Oflx and the size of nanocarriers. To quantitatively determine MIC$_{50}$, we fit the experimental data using an exponential decay equation ($y = ae^{-bx}$) with the highest regression and lowest error *via* MatLab. The MIC$_{50}$ of Oflx is defined as the concentration of Oflx required to reduce the growth of the cells by half. The results of MICs are summarized in Table 2, showing that the MICs of free Oflx and Oflx attached on nanocarriers highly depend upon the dose of Oflx and the size of nanocarriers.

Table 2 Study of dependence of MIC$_{50}$ of Oflx upon the size of nanocarriers in *E. coli* (WT)

Samples	MIC$_{50}$ of Oflx[a] (μM)
Free Oflx alone	0.144 ± 0.008
Nanocarriers (2.4 ± 0.7 nm)	0.314 ± 0.010
Nanocarriers (13.0 ± 3.1 nm)	0.081 ± 0.002
Nanocarriers (92.6 ± 4.4 nm)	0.026 ± 0.003

[a] The MIC of Oflx for each sample was determined by fitting the experimental data with the exponential decay ($y = ae^{-bx}$, inhibitory effects upon the exponential cell growth) to determine the parameters (a and b) of a fitting equation with a regression using MatLab. The equation was then used to determine the concentration of Oflx at which the cell growth was inhibited to the half of the cell growth of the blank control experiment, as described in Fig. 6 caption.

For free Oflx (Fig. 6D), the OD$_{600\ nm}$ of the cell suspension decreases with the increasing Oflx concentration, showing the MIC$_{50}$ of 0.144 ± 0.008 μM Oflx against the *E. coli* cells. Interestingly, the OD$_{600\ nm}$ of the cell suspension cultured with 2.4 ± 0.7 nm Oflx nanocarriers (Fig. 6E) decreases with the increasing Oflx concentration less rapidly than that for free Oflx and two other larger nanocarriers, showing the highest MIC$_{50}$ of 0.314 ± 0.010 μM Oflx and the lowest inhibitory effects against the *E. coli*. Notably, the OD$_{600\ nm}$ of the cell suspension cultured with 13.0 ± 3.1 nm Oflx nanocarriers (Fig. 6F) decreases with the increasing Oflx concentration more rapidly than that for free Oflx and 2.4 ± 0.7 nm Oflx nanocarriers, showing lower MIC$_{50}$ of 0.081 ± 0.002 and higher inhibitory effects against the *E. coli* cells than those of free Oflx and 2.4 ± 0.7 nm Oflx nanocarriers. Further, the OD$_{600\ nm}$ of the cell suspension cultured with 92.6 ± 4.4 nm nanocarriers (Fig. 6G) decreases with the increasing Oflx concentration most rapidly, showing the lowest MIC of 0.026 ± 0.003 Oflx and the highest inhibitory effects against the *E. coli* cells.

It is worth noting that the MIC$_{50}$ of Oflx nanocarriers highly depends upon their sizes. The largest size (92.6 ± 4.4 nm) nanocarriers exhibit the lowest MIC$_{50}$ and the highest inhibitory effects among the nanocarriers and free Oflx. In other words, the same amount of Oflx molecules loaded and delivered *via* the largest NPs (92.6 ± 4.4 nm) is the most potent, followed by 13.0 ± 3.1 nm nanocarriers, free Oflx, and 2.4 ± 0.7 nm nanocarriers (Table 2). The MIC$_{50}$ of conjugated Oflx of 2.4 ± 0.7 nm nanocarriers is more than two times higher than that of free drug Oflx. In contrast, the MIC$_{50}$ of 13.0 ± 3.1 nm and 92.6 ± 4.4 nm nanocarriers is nearly two times and 6 times lower than that of free Oflx, respectively. The highest number of Oflx molecules attached onto the largest nanocarriers could behave similarly to a planar surface (low particle curvature) leading to a larger contact surface area to create a high local concentration, which consequently favors formation of more drug binding sites.[60,61] These findings suggest that the densely packed Oflx molecules that are covalently linked with the self-assembled monolayer of MUNH$_2$ on the surface of the NPs could create multi-valence effects and enhance binding affinity of Oflx with target molecules and increase inhibitory effects.[62,63] Notably, the size-dependent inhibitory effects (MIC$_{50}$) of the nanocarriers are not

linearly proportional to their sizes, suggesting that it might have a trade-off role in inhibitory effects between the distribution of the same amount of the Oflx molecules throughout the cells and concentrating them on individual nanocarriers locally. Free Oflx and Oflx on smaller nanocarriers (2.4 ± 0.7 nm) might be distributed inside the cells more uniformly than the Oflx attached onto the larger nanocarriers (13.0 ± 3.1 nm and 92.6 ± 4.4 nm), while the larger nanocarriers offer higher local Oflx concentration and higher binding affinity with the target sites than the smaller nanocarriers. Considering the combination of Oflx distribution and binding affinity, an optimal size of nanocarriers could be designed to achieve the maximum antibiotic potency against given bacterial cells.

Size-dependent filamentation of *E. coli* using single live cell imaging

To investigate the mode of action of Oflx nanocarriers, we imaged the cells that had been cultured with free Oflx and Oflx nanocarriers over 18 h using dark-field optical microscopy. Representative optical images of the cells (Fig. 7B) incubated with (A) 0, (B) 0.045 μM free Oflx and 0.045 μM Oflx attached onto the nanocarriers with diameters of NPs of (C) 2.4 ± 0.7, (D) 13.0 ± 3.1 and (E) 92.6 ± 4.4 nm show that in the absence of Oflx (medium alone or AgMUNH$_2$ NPs), the *E. coli* cells grew normally and the average length of the cells was 1.8 ± 0.4 μm and no filamentous cells were observed (Fig. 7A), while the cells became filamentous in the presence of 0.045 μM free Oflx and Oflx nanocarriers (Fig. 7B–E). The percentage and length of filamentous cells highly depended upon the MIC$_{50}$ of Oflx and the size of the nanocarriers. 0.045 μM free Oflx generated 14.9% filamentous cells with an average length of cells at 3.8 ± 3.4 μm, ranging from 1.0 to 28.6 μm (Fig. 7B). Notably, the 0.045 μM Oflx nanocarriers of 2.4 ± 0.7, 13.0 ± 3.1 and 92.6 ± 4.4 nm (Fig. 7C–E) generated (C) 1.2% filamentous cells with an average length of 2.0 ± 0.9 μm, ranging from 1.1 to 11.4 μm; (D) 35% filamentous cells with an average length of 7.2 ± 8.7 μm, ranging from 1.4 to 57.0 μm; (E) 59% filamentous cells with an average length of 12.2 ± 12.1 μm, ranging from 1.7 to 73.8 μm, respectively. The results further demonstrate that the larger nanocarriers showed higher inhibitory effects and generated longer and a higher percentage of filamentous cells than the smaller nanocarriers. Interestingly, 2.4 ± 0.7 nm Oflx nanocarriers exhibited less inhibitory effect against the cells than free Oflx, and produced shorter and a lower percentage of filamentous cells than free Oflx, which is consistent with their MIC$_{50}$ in Fig. 5 and 6. Notably, the cells cultured with the largest nanocarriers (92.6 ± 4.4 nm) with the Oflx concentration higher than 0.045 μM did not grow and did not create a sufficient number of cells for statistics analysis.

Oflx is a fluoroquinolone antibiotic and has been commonly used to treat skin, bladder and urinary tract infection.[66,67] Its molecular target is DNA gyrase which is a crucial bacterial enzyme that catalyzes the negative supercoiling of double stranded DNA during cell replication.[66] Notably, Oflx can also partially inactivate D-alanine carboxypeptidases (enzymes that regulate the extent of peptide side-chain cross-linking in

peptidoglycan) and interfere with peptidoglycan biosynthesis, and bacterial filamentation in *E. coli*.[68–70] Notably, β-lactam antibiotics (*e.g.*, penicillin) and bacteriostatic antibiotics (*e.g.*, chloramphenicol) can generate filamentous cells.[71,72]

New findings

Our previous studies show the dose and size dependent inhibitory effects of antibiotic nanocarriers (AgMUNH–Oflx NPs) against *Pseudomonas aeruginosa* (Gram-negative bacterium) and *Bacillus subtilis* (Gram-positive bacterium).[45,46] Interestingly, inhibitory effects of antibiotic nanocarriers highly depend upon the expression of MexAB-OprM (multidrug membrane transporter) in *Pseudomonas aeruginosa*,[46] but not the expression of BmrA (multidrug ABC membrane transporter) in *Bacillus subtilis*.[45] This study shows that the inhibitory effects of nanocarriers against *E. coli* (Gram-negative bacterium) highly depend upon the dose and size of nanocarriers and the efflux function of ABC transporters in *E. coli*. This study shows that the mode of action of nanocarriers against *E. coli* is bactericidal effects that cause cellular filamentation, which highly depends upon the dose and size of nanocarriers. Notably, we did not observe any cell filamentation when *Pseudomonas aeruginosa* or *Bacillus subtilis* cells were cultured with the nanocarriers, as we reported previously.[45,46] These findings indicate that the modes of action of Oflx nanocarriers could highly depend upon the sizes of nanocarriers and the bacterial strain.

Notably, the MIC$_{50}$ values of free Oflx and the Oflx nanocarriers (2.4 ± 0.7, 13.0 ± 3.1 and 92.6 ± 4.4 nm) against *E. coli* are $4\times$, $3\times$, $5\times$, and $4\times$ lower than those against *P. aeruginosa* (WT), respectively.[46] Interestingly, the MIC$_{50}$ values of free Oflx and Oflx attached on nanocarriers (2.4 ± 0.7 nm) against *E. coli* are nearly the same as those against BmrA (WT, *B. subtilis*),[45] while the MIC$_{50}$ values of Oflx nanocarriers (13.0 ± 3.1 and 92.6 ± 4.4 nm) against *E. coli* are two times lower and two times higher than those against BmrA (WT, *B. subtilis*), respectively. The dose and size dependent inhibitory effects of Oflx nanocarriers against bacterial strains could be attributed to the combination of several factors such as their permeability into the bacterial cells and the efflux function of membrane transporters in extruding nanocarriers out of cells.[22,64] We have observed Oflx nanocarriers inside the cells and have used Oflx nanocarriers to study the efflux function of ABC transporters in single live cells.[65] Further studies are needed to depict the underlying molecular mechanisms. These new findings demonstrate the importance of using the same nanocarriers and same experimental methods to study their effects on different bacterial strains in order to determine the dependence of effects of nanocarriers against different membrane transporters and different bacterial strains. We cannot extrapolate these new findings from the previous studies.

Summary

In summary, we have successfully characterized and used three different sized antibiotic (Oflx) nanocarriers to study their dose and size-dependent inhibitory effects against *E. coli*. We have

designed a modified LB medium to culture the cells and enable the nanocarriers with desired concentrations to be stable (non-aggregated) in the medium over time (18 h) during the cell culture. Therefore, the dose and size of the nanocarriers remain unchanged over time, which enables us to study their dose and size dependent inhibitory effects against the *E. coli* cells and compare these new findings with those from our previous studies.[45,46] We found that the inhibitory effects of Oflx nanocarriers against the *E. coli* increase as the dose of Oflx and the size of nanocarriers increase. The largest nanocarriers (92.6 ± 4.4 nm) show the highest inhibitory effect and the lowest MIC_{50} (0.026 ± 0.003 μM) while the smallest nanocarriers (2.4 ± 0.7 nm) exhibit the lowest inhibitory effect and the highest MIC_{50} (0.314 ± 0.010 μM) against *E. coli*. These results demonstrate that inhibitory potency of the same amount of Oflx molecules could substantially increase when they are carried and delivered by the larger nanocarriers, suggesting that the densely packed Oflx molecules on the NPs might have offered multivalence effects, which augments the binding affinity and increases local drug concentrations, leading to higher potency. Further, our results show the size-dependent effect of Oflx nanocarriers on cellular filamentation, leading to bacterial death, and that the larger nanocarriers create longer and higher percentage of filamentous cells than the smaller nanocarriers. Notably, the inhibitory effect and bactericidal effect of the smallest nanocarriers (2.4 ± 0.7 nm) are less than free Oflx, suggesting that the combination of the multivalence effect and their intracellular distribution could both play roles in their inhibitory effects against the cell growth. These results show that the inhibitory effects of nanocarriers are not linearly proportional to their sizes, and the optimal-sized nanocarriers could be designed to create the most potent effect of antibiotic nanocarriers. Efforts are in progress to further characterize the underlying molecular mechanisms of size-dependent inhibitory effects of nanocarriers against bacteria.

Conflicts of interest

There are no conflicts to declare.

Abbreviations

$MUNH_2$	11-Amino-1-undecanethiol
EDC	1-Ethyl-3-[3-dimethylaminopropyl]-carbodiimide hydrochloride
ABC	ATP-binding cassette
DFOMS	Dark-field optical microscopy and spectroscopy
DI	Deionized
DLS	dynamic light scattering
E. coli	*Escherichia coli*
HRTEM	High-resolution transmission electron microscopy
h:	Hour
LSPR	Localized surface plasmon resonance
MIC_{50}	Minimum inhibitory concentration
MDR	Multidrug resistance
nm	Nanometer
NP	Nanoparticle
Sulfo-NHS	*N*-Hydroxysulfosuccinimide
Oflx	Ofloxacin
$OD_{600 nm}$	Optical density at 600 nm
Ag NPs	Silver nanoparticles

References

1 S. P. Cole, *J. Biol. Chem.*, 2014, **289**, 30880–30888.
2 J. I. Fletcher, R. T. Williams, M. J. Henderson, M. D. Norris and M. Haber, *Drug Resist. Updates*, 2016, **2**, 1–9.
3 K. McIntosh, C. Balch and A. K. Tiwari, *Expert Opin. Drug Metab. Toxicol.*, 2016, **12**, 633–644.
4 R. W. Robey, K. M. Pluchino, M. D. Hall, A. T. Fojo, S. E. Bates and M. M. Gottesman, *Nat. Rev. Cancer*, 2018, **18**, 452–464.
5 C. F. Higgins and K. J. Linton, *Nat. Struct. Mol. Biol.*, 2004, **11**, 918–926.
6 G. Chang, *FEBS Lett.*, 2003, **555**, 102–105.
7 S. K. Nigam, *Nat. Rev. Drug Discovery*, 2015, **14**, 29–44.
8 S. Trowitzsch and R. Tampé, *J. Mol. Biol.*, 2018, **430**, 4481–4495.
9 O. Olsvik, Y. Wasteson, A. Lund and E. Hornes, *Int. J. Food Microbiol.*, 1991, **12**, 103–113.
10 A. L. Flores-Mireles, J. N. Walker, M. Caparon and S. J. Hultgren, *Nat. Rev. Microbiol.*, 2015, **13**, 269–284.
11 W. T. Doerrler and C. R. Raetz, *J. Biol. Chem.*, 2002, **277**, 36697–36705.
12 P. D. Eckford and F. J. Sharom, *J. Biol. Chem.*, 2008, **283**, 12840–12850.
13 G. Chang and C. B. Roth, *Science*, 2001, **293**, 1793–1800.
14 M. M. Gottesman, S. V. Ambudkar and D. Xia, *Nat. Biotechnol.*, 2009, **27**, 546–547.
15 C. F. Higgins, *Res. Microbiol.*, 2001, **152**, 205–210.
16 L. W. Hung, I. X. Wang, K. Nikaido, P. Q. Liu, G. F. Ames and S. H. Kim, *Nature*, 1998, **396**, 703–707.
17 A. L. Davidson and J. Chen, *Annu. Rev. Biochem.*, 2004, **73**, 241–268.
18 R. J. Dawson and K. P. Locher, *Nature*, 2006, **443**, 180–185.
19 S. Mishra, B. Verhalen, R. A. Stein, P. C. Wen, E. Tajkhorshid and H. S. Mchaourab, *eLife*, 2014, **3**, e0274.
20 P. M. Jones and A. M. George, *Crit. Rev. Biochem. Mol. Biol.*, 2013, **48**, 39–50.
21 H. Singh, S. Velamakanni, M. J. Deery, J. Howard, S. L. Wei and H. W. van Veen, *Nat. Commun.*, 2016, **7**, 12387.
22 A. S. Skwarecki, S. Milewski, M. Schielmann and M. J. Milewska, *Nanomedicine*, 2016, **12**, 2215–2240.

23 R. Y. Pelgrift and A. J. Friedman, *Adv. Drug Deliv. Rev.*, 2013, **65**, 1803–1815.

24 V. Van Giau, S. An and J. Hulme, *Drug Des., Dev. Ther.*, 2019, **13**, 327–343.

25 D. Y. Wang, H. C. van der Mei, Y. Ren, H. J. Busscher and L. Shi, *Front. Chem.*, 2020, **7**, 872.

26 S. V. Kyriacou, *Real-time Study of Multidrug Resistance Mechanism in Pseudomonas aeruginosa Using Nanoparticle Optics and Single Live Cell Imaging*, Old Dominion University, thesis, 2003.

27 D. Lv, R. Wang, G. Tang, Z. Mou, J. Lei, J. Han, S. De Smedt, R. Xiong and C. Huang, *ACS Appl. Mater. Interfaces*, 2019, **11**, 12880–12889.

28 P. D. Nallathamby, T. Huang and X.-H. N. Xu, *Nanoscale*, 2010, **2**, 1715–1722.

29 K. J. Lee, L. M. Browning, T. Huang, F. Ding, P. D. Nallathamby and X.-H. N. Xu, *Anal. Bioanal. Chem.*, 2010, **397**, 3317–3328.

30 P. D. Nallathamby, K. J. Lee, T. Desai and X.-H. N. Xu, *Biochemistry*, 2010, **49**, 5942–5953.

31 X.-H. N. Xu, W. J. Brownlow, S. V. Kyriacou, Q. Wan and J. J. Viola, *Biochemistry*, 2004, **43**, 10400–10413.

32 X.-H. N. Xu, J. Chen, R. B. Jeffers and S. V. Kyriacou, *Nano Lett.*, 2002, **2**, 175–182.

33 T. Huang, L. M. Browning and X.-H. N. Xu, *Nanoscale*, 2012, **4**, 2797–2812.

34 T. Huang, P. D. Nallathamby, D. Gillet and X.-H. N. Xu, *Anal. Chem.*, 2007, **79**, 7708–7718.

35 K. J. Lee, P. D. Nallathamby, L. M. Browning, C. J. Osgood and X.-H. N. Xu, *ACS Nano*, 2007, **1**, 133–143.

36 K. J. Lee, P. D. Nallathamby, L. M. Browning, T. Desai, P. Cherukuri and X.-H. N. Xu, *Analyst*, 2012, **137**, 2973–2986.

37 P. D. Nallathamby, K. J. Lee and X.-H. N. Xu, *ACS Nano*, 2008, **2**, 1371–1380.

38 P. D. Nallathamby and X.-H. N. Xu, *Nanoscale*, 2010, **2**, 942–952.

39 L. M. Browning, K. J. Lee, P. K. Cherukuri, P. D. Nallathamby, S. Warren, J.-M. Jault and X.-H. N. Xu, *RSC Adv.*, 2016, **6**, 36794–36802.

40 L. M. Browning, K. J. Lee, P. K. Cherukuri, T. Huang, S. Warren and X.-H. N. Xu, *J. Phys. Chem. C*, 2016, **120**, 21007–21016.

41 L. M. Browning, K. J. Lee, T. Huang, P. D. Nallathamby, J. Lowman and X.-H. N. Xu, *Nanoscale*, 2009, **1**, 138–152.

42 L. M. Browning, K. J. Lee, P. K. Cherukuri, T. Huang, P. Songkiatisak, S. Warren and X. Xu, *Analyst*, 2018, **143**, 1599–1608.

43 X.-H. N. Xu, in *Encyclopedia of Spectroscopy and Spectrometry*, ed. J. Lindon, G. E. Tranter and D. Koppenaal, Elsevier, Oxford, Third edn, 2017, vol. 1, pp. 566–570.

44 X.-H. N. Xu, Y. Song and P. D. Nallathamby, in *New Frontiers in Ultrasensitive Bioanalysis: Advanced Analytical Chemistry Applications in Nanobiotechnology, Single Molecule Detection, and Single Cell Analysis*, ed. X.-H. N. Xu, Wiley, New Jersey, 2007, pp. 41–65.

45 P. K. Cherukuri, P. Songkiatisak, F. Ding, J. M. Jault and X. Xu, *ACS Omega*, 2020, **5**, 1625–1633.

46 F. Ding, P. Songkiatisak, P. K. Cherukuri, T. Huang and X. Xu, *ACS Omega*, 2018, **3**, 1231–1243.

47 T. Huang, P. D. Nallathamby and X.-H. N. Xu, *J. Am. Chem. Soc.*, 2008, **130**, 17095–17105.

48 T. Huang and X.-H. N. Xu, *J. Mater. Chem.*, 2010, **20**, 9867–9876.

49 M. Berney, F. Hammes, F. Bosshard, H. U. Weilenmann and T. Egli, *Appl. Environ. Microbiol.*, 2007, **73**, 3283–3290.

50 F. Ding, K. Lee, A. Vahedi-Faridi, T. Huang and X.-H. N. Xu, *Anal. Bioanal. Chem.*, 2011, **400**, 223–235.

51 E. Steinfels, C. Orelle, J. R. Fantino, O. Dalmas, J. L. Rigaud, F. Denizot, A. Di Pietro and J. M. Jault, *Biochemistry*, 2004, **43**, 7491–7502.

52 J. Tolls, *Environ. Sci. Technol.*, 2001, **35**, 3397–3406.

53 Y. Hochman, S. Carmeli and C. Carmeli, *J. Biol. Chem.*, 1993, **268**, 12373–12379.

54 I. L. Urbatsch, G. A. Tyndall, G. Tombline and A. E. Senior, *J. Biol. Chem.*, 2003, **278**, 23171–23179.

55 G. Cosa, K.-S. Focsaneanu, J. R. N. McLean, J. P. McNamee and J. C. Scaiano, *Photochem. Photobiol.*, 2001, **73**, 585–599.

56 X.-H. N. Xu, S. Kyriacou and R. Jeffers, Metallic Nanoparticles for Inhibition of Bacterium Growth, *US Pat.* App. US20030108612A1, 2002.

57 K. J. Lee, L. M. Browning, P. D. Nallathamby and X. H. N. Xu, *Chem. Res. Toxicol.*, 2013, **26**, 904–917.

58 L. M. Browning, T. Huang and X.-H. N. Xu, *Interface Focus*, 2013, **3**, 20120098.

59 S. V. Kyriacou, W. J. Brownlow and X. H. N. Xu, *Biochemistry*, 2004, **43**, 140–147.

60 H. D. Hill, J. E. Millstone, M. J. Banholzer and C. A. Mirkin, *ACS Nano*, 2009, **3**, 418–424.

61 A. Mulder, J. Huskens and D. N. Reinhoudt, *Org. Biomol. Chem.*, 2004, **2**, 3409–3424.

62 H. Gu, P. L. Ho, E. Tong, L. Wang and B. Xu, *Nano Lett.*, 2003, **3**, 1261–1263.

63 L. Vigderman and E. R. Zubarev, *Adv. Drug Delivery Rev.*, 2013, **65**, 663–676.

64 C. McCaffrey, A. Bertasso, J. Pace and N. H. Georgopapadakou, *Antimicrob. Agents Chemother.*, 1992, **36**, 1601–1605.

65 P. Songkiatisak, *Study of ABC membrane transporter in single live cells*, Old Dominion University, Dissertation, 2018.

66 W. A. J. Petri, in *Goodman & Gilman's The phamacological basis of therapeutics*, ed. L. L. Brunton, The McGraw-Hill, 12th edn, 2011, ch. 52, pp. 1463–1476.

67 P. A. Todd and D. Faulds, *Drugs*, 1991, **42**, 825–876.

68 M. Tanaka, M. Otsuki and T. Nishino, *J. Antimicrob. Chemother.*, 1992, **26**, 659–666.

69 D. Mirelman, Y. Yashouv-Gan and U. Schwarz, *J. Bacteriol.*, 1977, **129**, 1593–1600.

70 S. Vincent, B. Glauner and L. Gutmann, *Antimicrob. Agents Chemother.*, 1991, **35**, 1381–1385.

71 T. Horii, M. Kobayashi, K. Sato, S. Ichiyama and M. Ohta, *J. Antimicrob. Chemother.*, 1998, **41**, 435–442.

72 C. Steel, Q. Wan and X. H. Xu, *Biochemistry*, 2004, **43**, 175–182.